Finite element model for carbon nanotube-reinforced and graphene nanoplatelet-reinforced composite beams

Armagan Karamanli[a,*], Thuc P. Vo[b]

[a]Faculty of Engineering and Natural Sciences, Mechatronics Engineering, Bahcesehir University, Istanbul, Turkey.

[b]School of Engineering and Mathematical Sciences, La Trobe University, Bundoora, VIC 3086, Australia

[*]Corresponding author. E-mail: armaganfatih.karamanli@eng.bau.edu.tr (A. Karamanli)

Abstract

This paper investigates bending, vibration and buckling analysis of carbon nanotube-reinforced composite (CNTRC) and graphene nanoplatelet-reinforced composite (GPLRC) beams. Both normal and shear effects are included in the formulation of the governing equations of motion of the beams. Finite element model is employed to determine displacements, critical buckling loads and natural frequencies of the beams with different boundary conditions. Several important factors in parametric studies including distribution pattern, volume fraction of CNTs, GPL weight fraction, slenderness ratio, boundary condition, etc. are investigated. Some new results are given as benchmark for further validation.

Keywords: CNTRC; GPLRC; FEM; bending; vibration; buckling

1. Introduction

Carbon nanotubes (CNTs) and Graphene Platelets (GPLs) are considered one of the most excellent candidates for the reinforcement of polymer composites due to their extremely attractive mechanical properties such as high Young's modulus, tensile strength and low density [1-3]. The potential applications of carbon nanotube reinforced composites (CNTRCs) and graphene platelets (GPLs) reinforced composites (GPLRCs) can be found in the field of high-performance structures and multifunctional composites. The constitutive models and mechanical properties of CNTRCs have been studied experimentally [4, 5] and numerically [6-9]. In order to improve the interfacial bonding strength, the use of the functionally graded material (FGM) concept for producing CNTRC [10] and GPLRC [11] structures is proposed. In the practical applications, CNTRCs/GPLRCs may be incorporated in the form of structural components such as beams, plates and shells [12, 13]. The prediction of structural behaviours of CNTRCs/GPLRCs beams is therefore necessary. Yang, Kitipornchai and co-workers employed classical beam theory (CBT) and First order beam theory (FBT) to study linear (vibration, buckling) and nonlinear responses (bending, buckling) of CNTRC beams [14-19] and GPLRCs beams [20-23]. FBT was further employed to investigate the free vibration and buckling analysis of CNTRC beams by Yas et al. [24-26], Wattanasakulpong and Mao [27] and their nonlinear dynamic responses by Ansari et al. [28]. It should be noted that FBT requires shear correction factor, whose the correct value is difficult to determine. In order to avoid this issue, the higher-order beam theories (HBTs) should be used. Wattanasakulpong and Ungbhakorn [29] proposed Navier solutions for several HBTs to study vibration, buckling and bending responses of CNTRC beams on an elastic foundation. Lin and Xiang [30] studied dynamic responses of CNTRC beams by using both FBT and third-order beam theory (TBT). Shen et al. [31] extended their previous HBT [10] to study nonlinear behaviours of GPLRCs beams and solved by two-step perturbation technique. Anirudh et al. [32] used trigonometric

beam theory to study GPLRCs curved beams by using finite element model. Barati and Zenkour [33] used refined beam theory to study post-buckling responses of GPLRCs beams. It should be noted that the HBTs in above studies [29-33] neglecting the thickness stretching effect, which needs to be considered to fulfil Koiter's recommendation [34]. This effect is very important for FG structures [35, 36] especially for thick beams and needs to be taken into account.

In order to include the thickness stretching effect, this paper uses shear and normal deformation theory (SNDT) to investigate the bending, buckling and free vibration analyses of CNTRC and GPLRC beams. Material properties are assumed to be uniformly or FG distribution through the thickness. Equations of motion and boundary conditions of the present theory are derived from Hamilton's principle. Numerical examples are presented to verify accuracy of present theory and investigate the effects of distribution pattern, and volume fraction of CNTs, GPL weight fraction, slenderness ratio, boundary conditions on deflections, buckling loads and natural frequencies.

2. Theoretical Formulation

The problem domain of this study can be described as a straight beam with length (L), height (h) and width (b) as shown in Fig. 1. Two different material properties, namely, CNTRC and GPLRC beams are considered.

Figure 1 About Here

2.1 Material properties of CNTRC beams

The CNTRC beams are made of a mixture of CNTs and an isotropic matrix. Based on the distribution pattern of CNTs, there are four different models available in the open literature, namely, UD – CNTRC, V – CNTRC, O – CNTRC and X – CNTRC as shown in Fig. 2.

Figure 2 About Here

The volume fractions of CNTs in the forementioned models are given by [37];

$$VV_{CCCCCC}(zz) = \begin{cases} VV^{*}_{CCCCC} & UUUU - CCCCCCCCCC \\ VV^{*}_{CCCCCC}\left(1 + \frac{2zz}{h}\right) & VV - CCCCCCCCCC \\ VV^{*}_{CCCCCC}\left(2 - \frac{4|zz|}{h}\right) & OO - CCCCCCCCCC \\ VV^{*}_{CCCCCC}\left(\frac{4|zz|}{h}\right) & XX - CCCCCCCCCC \end{cases} \quad (1aa)$$

$$VV^{*}_{CCCCCC} = \frac{WW_{CCCCCC}}{WW_{CCCCCC} + (\rho\rho_{CCCCCC}/\rho\rho_{mm}) - (\rho\rho_{CCCCCC}/\rho\rho_{mm})WW_{CCCCCC}} \quad (1bb)$$

where WW_{CCCCCC} , $\rho\rho_{CCCCCC}$ are the mass fraction and density of CNTs, $\rho\rho_{mm}$ is the mass density of the polymer matrix.

The effective material properties of the CNTRC beams are calculated by the rule of mixture [10] via Young's and shear modulus of CNT (EE^{CCCCCC}_{11},EE^{CCCCCC}_{22}, GG^{CCCCCC}_{12}) and those of polymer matrix (EE_{mm}, GG_{mm}):

$$EE_{11} = \eta_1 W_{CCCCCC} EE^{CCCCCC}_{1} + V_{mm} EE_{mm} \quad (2aa)$$

$$\frac{\eta_2}{EE_{22}} = \frac{VV_{CCCCCC}}{EE^{CCCCCC}_{2}} + \frac{VV_{mm}}{EE_{mm}} \quad (2bb)$$

$$\frac{\eta_3}{GG_{12}} = \frac{VV_{CCCCCC}}{GG^{CCCCCC}_{1}} + \frac{VV_{mm}}{GG_{mm}} \quad (2cc)$$

where the η_1, η_2 and η_3 define the CNT efficiency parameters and W_{CCCCCC} and V_m are the volume fractions of CNT and polymer matrix:

$$VV_{CCCCCC} + VV_{mm} = 1 \tag{3}$$

The Poisson's ratio and mass density of the CNTRC beams can be calculated via Poisson's ratio of the CNTs (vv_{CCCCCC}) and polymer matrix (vv_{mm}) [37]:

$$vv = W_{CCCCCC} vv_{CCCCCC} + V_m vv_{mm} \tag{4aa}$$

$$\rho\rho = W_{CCCCCC} \rho\rho_{CCCCCC} + V_m \rho\rho_{mm} \tag{4cc}$$

For the analysis, the following CNT efficiency parameters are used [24]:

$$VV^*_{CCCCC} = 0.12;\ \eta_1 = 1.2833;\ \eta_2 = \eta_3 = 1.0556 \tag{5aa}$$

$$VV^*_{CCCCC} = 0.17;\ \eta_1 = 1.3414;\ \eta_2 = \eta_3 = 1.7101 \tag{5bb}$$

$$VV^*_{CCCCC} = 0.28;\ \eta_1 = 1.3238;\ \eta_2 = \eta_3 = 1.7380 \tag{5cc}$$

2.2 Material properties of GPLRC beams

GPLRC beams can be defined as a mixture of GPLs and polymer matrix. The layers of the GPLs which are designed with the same thickness, are perfectly bounded each other. The volume fractions of GPLs in the forementioned models are given by [21] as shown in Fig. 3;

$$W_{GGGGGG}(kk) = \begin{cases} VV^*_{GGGGGG} & UU - GGGGGGCCCC \\ dd_{GGGG} \dfrac{(2kk-1)}{CC_{GG}} & AA - GGGGGGCCCC \\ 2VV^*_{GGGGGG}\left(1 - \dfrac{|2kk - CC_{GG} - 1|}{CC_{GG}}\right) & OO - GGGGGGCCCC \\ 2VV^*_{dd_{GGGG}} \dfrac{|2kk - CC_{GG} - 1|}{CC_{GG}} & XX - GGGGGGCCCC \end{cases} \tag{6aa}$$

$$VV^*_{GGGGGG} = \frac{WW_{GGGGGG}}{WW_{GGGGGG} + (\rho\rho_{GGGGGG}/\rho\rho_{mm})(1 - WW_{GGGGGG})} \tag{6bb}$$

where, VV^{*}_{GGGGGG} is the total volume fraction of GPLs, CC_{GG} $(kk = 1,2,3,..,CC_{GG})$ is the total number of layers, $\rho\rho_{GGGGGG}$ is the mass density of GPL.

Figure 3 About Here

The effective elastic moduli of a GPL layer can be computed by [21]:

$$EE = \frac{3}{8}\frac{1+\xi\xi_{GG}\eta\eta_{GG}VV_{GGGGGG}}{1-\eta\eta_{GG}VV_{GGGGGG}}EE_{mm} + \frac{5}{8}\frac{1+\xi\xi_{CC}\eta\eta_{CC}VV_{GGGGGG}}{1-\eta\eta_{CC}VV_{GGGGGG}}EE_{mm} \quad (7aa)$$

$$\eta\eta_{GG} = \frac{(EE_{GGGGGG}/EE_{mm})-1}{(E_{GGGGGG}/EE_{mm})+\xi\xi_{GG}} \quad (7bb)$$

$$\eta\eta_{CC} = \frac{(EE_{GGGGGG}/EE_{mm})-1}{(E_{GGGGGG}/EE_{mm})+\xi\xi_{CC}} \quad (7cc)$$

$$\xi\xi_{GG} = 2\left(\frac{aa_{GGGGGG}}{tt_{GGGGGG}}\right) \quad (7dd)$$

$$\xi\xi_{CC} = 2\left(\frac{bb_{GGGGGG}}{tt_{GGGGGG}}\right) \quad (7ee)$$

$$\xi\xi_{GG} = 2\left(\frac{aa_{GGGGGG}}{bb_{GGGGGG}}\right)\left(\frac{bb_{GGGGGG}}{tt_{GGGGGG}}\right) \quad (7ff)$$

where, EE_{GGGGGG} is the Young's modulus of GPL. aa_{GGGGGG}, bb_{GGGGGG} and tt_{GGGGGG} are the length, width and thickness of GPL. The aspect and width to thickness ratios of GPL can be expressed by:

$$\left(\frac{aa_{GGGGGG}}{bb_{GGGGGG}}\right) \text{ and } \left(\frac{bb_{GGGGGG}}{tt_{GGGGGG}}\right) \quad (8)$$

The Poisson's ratio and mass density of the GPLRC beams can be calculated via Poisson's ratio of the GPL (ν_{GGGGGG}) and polymer matrix (ν_{mm}):

$$\nu\nu = \nu\nu_{mm}(1 - W_{GGGGGG}) + \nu\nu_{GGGGGG}W_{GGGGGG} \tag{9aa}$$

$$\rho\rho = \rho\rho_{mm}(1 - W_{GGGGGG}) + \rho\rho_{GGGGGG}W_{GGGGGG} \tag{9bb}$$

2.3 Variational Formulation

The following shear and normal deformation theory (SNDT) is used to represent the displacement field [38-41]:

$$uu_1(xx, zz, tt) = UU(xx, zz, tt) = uu(xx, tt) - ff_1(zz)\frac{\partial\partial ww_{bb}(xx, tt)}{\partial\partial xx} + ff_2(zz)\frac{\partial\partial ww_{ss}(xx, tt)}{\partial\partial xx} \tag{10aa}$$

$$uu_3(xx, tt) = WW(xx, tt) = ww_{bb}(xx, tt) + ww_{ss}(xx, tt) + ff_3(zz)\, ww_{zz}(xx, tt) \tag{10bb}$$

$$ff_1(zz) = \frac{4zz^3}{3h^2}, ff_2(zz) = zz - \frac{8zz^3}{3h^2}\ aaaadd\ \ ff_3(zz) = 1 - \frac{4zz^2}{h^2} \tag{10cc}$$

where $uu, ww_{bb}, ww_{ss}\ aaaadd\ ww_{zz}$ are unknowns of the displacement field.

The strains associated with the SNDT are given by:

$$\varepsilon\varepsilon_{xx} = \frac{\partial\partial UU}{\partial\partial xx} = uu' - ff_1\, ww_{bb}'' + ff_2\, ww_{ss}'' \tag{11aa}$$

$$\varepsilon\varepsilon_{zz} = \frac{\partial\partial WW}{\partial\partial zz} = ff_3'\, ww_{zz} \tag{11bb}$$

$$\gamma\gamma_{xxzz} = \frac{\partial\partial WW}{\partial\partial xx} + \frac{\partial\partial UU}{\partial\partial zz} = ff_3(ww_{bb}' + 2ww_{ss}' + ww_{zz}') \tag{11cc}$$

Constitutive relations between stresses and strains based on the CNTRC and GPLRC beams can be obtained in the form of:

$$\begin{Bmatrix}\sigma\sigma_{xx}\\ \sigma\sigma_{zz}\\ \sigma\sigma_{xxzz}\end{Bmatrix} = \begin{bmatrix}QQ_{11} & QQ_{13} & 0\\ QQ_{13} & QQ_{33} & 0\\ 0 & 0 & QQ_{44}\end{bmatrix}\begin{Bmatrix}\varepsilon\varepsilon_{xx}\\ \varepsilon\varepsilon_{zz}\\ \gamma\gamma_{xxzz}\end{Bmatrix} \tag{12aa}$$

$$QQ_{11}(zz) = QQ_{33}(zz) = \frac{EE_{11}(zz)}{1 - \nu\nu^2(zz)} \tag{12bb}$$

$$QQ_{13}(zz) = \frac{EE_{22}(zz)vv(zz)}{\left(1 - vv^2(zz)\right)} \tag{12cc}$$

$$QQ_{44}(zz) = GG_{12}(zz) \tag{12dd}$$

Using the SNDT given in Eq. (10), the strain energy ($\mathcal{UU}$) is expressed by:

$$\mathcal{UU} = \frac{1}{2}\int_{VV}(\sigma\sigma_{xx}\varepsilon\varepsilon_{xx} + \sigma\sigma_{zz}\varepsilon\varepsilon_{zz} + \sigma\sigma_{xxzz}\gamma\gamma_{xxzz})ddVV \tag{13aa}$$

$$\mathcal{UU} = \frac{1}{2}\int_{VV}[(\varepsilon\varepsilon_{11xx}^{2} + 2QQ_{13}\varepsilon\varepsilon_{xx}\varepsilon\varepsilon_{zz} + QQ_{11zz}\varepsilon\varepsilon_{zz}^{2} + \gamma\gamma_{44xxzz}^{2})]ddVV \tag{13bb}$$

The work (VV) done by the uniformly load q(x) and axial force CC_0 is given by:

$$VV = -\frac{1}{2}\int_0^{GG} CC_0\left(\frac{\partial ww_{bb}}{\partial xx}\right)^2 + \left(\frac{\partial ww_{ss}}{\partial xx}\right)^2 + \left(\frac{\partial ww_{zz}}{\partial xx}\right)^2 + 2\frac{\partial ww_{bb}}{\partial xx}\frac{\partial ww_{ss}}{\partial xx} + 2\frac{\partial ww_{bb}}{\partial xx}\frac{\partial ww_{zz}}{\partial xx} + +2\frac{\partial ww_{ss}}{\partial xx}\frac{\partial ww_{zz}}{\partial xx}\Big)ddxx -$$

$$\int_{bb}^{GG}\{qq(ww_{ss} + ww_{zz} + ff_3(zz)ww_{zz}\}ddxx \tag{14}$$

The kinetic energy (KK) is derived by:

$$KK = \frac{1}{2}\int_{VV}\rho\rho(uui_1^2 + uui_3^2)ddVV \tag{15aa}$$

$$KK = \frac{1}{2}\int_0^{GG}\left(II_0\left(\frac{\partial uu}{\partial tt}\right)^2 + \left(\frac{\partial ww_{bb}}{\partial tt}\right)^2 + \left(\frac{\partial ww_{ss}}{\partial tt}\right)^2 + 2\left(\frac{\partial ww_{bb}}{\partial tt}\right)\left(\frac{\partial ww_{ss}}{\partial tt}\right) - 2II_1\left(\frac{\partial uu}{\partial tt}\right)\left(\frac{\partial^2 ww_{bb}}{\partial xx\partial tt}\right) + II_2\left(\frac{\partial^2 ww_{bb}}{\partial xx\partial tt}\right)^2\right.$$

$$+ 2JJ_1\left(\frac{\partial uu}{\partial tt}\right)\left(\frac{\partial^2 ww_{ss}}{\partial xx\partial tt}\right) + 2JJ_2\left(\frac{\partial ww_{bb}}{\partial tt}\right)\left(\frac{\partial ww_{zz}}{\partial tt}\right) + \left(\frac{\partial ww_{ss}}{\partial tt}\right)\left(\frac{\partial ww_{zz}}{\partial tt}\right) - 2JJ_3\left(\frac{\partial^2 ww_{bb}}{\partial xx\partial tt}\right)\left(\frac{\partial^2 ww_{ss}}{\partial xx\partial tt}\right)$$

$$\left. + KK_1\left(\frac{\partial^2 ww_{ss}}{\partial xx\partial tt}\right)^2 + KK_2\left(\frac{\partial ww_{zz}}{\partial tt}\right)^2\right)ddxx \tag{15bb}$$

where t is the time and the inertial coefficients can be expressed as:

$$(II_0, II_1, II_2, JJ_1, JJ_2, JJ_3, KK_1, KK_2) = \int_{-\frac{h}{2}}^{+\frac{h}{2}}\rho\rho\left(1, ff_1, ff_1^2, ff_2, ff_3, ff_1ff_2, ff_2^2, ff_3^2\right)ddz \tag{16}$$

2.4 Finite Element Modelling

The shape functions for the unknown elements of the displacement field; $uu(xx,tt)$, $ww_{bb}(xx,tt)$, $ww_{ss}(xx,tt)$ and $ww_{zz}(xx,tt)$, are determined based on the strain energy function by employing a two-node beam element in the form of:

$$uu(xx,tt) = \sum_{jj=1}^{4} uu_{jj}\,\varphi\varphi_{jj}(xx)\,ee^{ii\,ii\,tt}, \tag{17aa}$$

$$ww_{bb}(xx,tt) = \sum_{jj=1}^{4} ww_{bb_j}\,\varphi\varphi_{jj}(xx)\,ee^{ii\,ii\,tt}, \tag{17bb}$$

$$ww_{ss}(xx,tt) = \sum_{jj=1}^{4} ww_{ss_j}\,\varphi\varphi_{jj}(xx)\,ee^{ii\,ii\,tt}, \tag{17cc}$$

$$ww_{zz}(xx,tt) = \sum_{jj=1}^{4} ww_{zz_j}\,\varphi\varphi_{jj}(xx)\,ee^{ii\,ii\,tt}, \tag{17dd}$$

Above, the natural frequency is expressed by $\omega\omega$.

The unknows per element are defined by:

$$uu_{jj} = \left[uu^{(1)}, uu_{,xx}^{(1)}, uu^{(2)}, uu_{,xx}^{(2)}\right] \tag{18aa}$$

$$ww_{bb\,jj} = \left[ww_{bb}^{(1)}, ww_{bb\,,xx}^{(1)}, ww_{bb}^{(2)}, ww_{bb\,,xx}^{(2)}\right] \tag{18bb}$$

$$ww_{ss\,jj} = \left[ww_{ss}^{(1)}, ww_{ss\,,xx}^{(1)}, ww_{ss}^{(2)}, ww_{ss\,,xx}^{(2)}\right] \tag{18cc}$$

$$ww_{zz\,jj} = \left[ww_{zz}^{(1)}, ww_{zz\,,xx}^{(1)}, ww_{zz}^{(2)}, ww_{zz\,,xx}^{(2)}\right] \tag{18dd}$$

Shape functions of a two-node beam element are:

$$\varphi\varphi_1(xx) = 1 - \frac{3xx^2}{ll^2} + \frac{2xx^3}{ll^3} \tag{19aa}$$

$$\varphi\varphi_2(xx) = xx - \frac{2xx^2}{ll} + \frac{xx^3}{ll^2} \tag{19bb}$$

$$\varphi\varphi_3(xx) = \frac{3xx^2}{ll^2} - \frac{2xx^3}{ll^3} \tag{19cc}$$

$$\varphi\varphi_4(xx) = -\frac{xx^2}{ll} + \frac{xx^3}{ll^2} \tag{19dd}$$

To compute the unknown variables, the Lagrange's equations method is used by using the energy functional (Π).

$$\Pi = UU + VV - KK \tag{20aa}$$

$$\frac{\partial\partial\Pi}{\partial\partial uu_{jj}} = 0, \quad \frac{\partial\partial\Pi}{\partial\partial ww_{bb_{jj}}} = 0, \quad \frac{\partial\partial\Pi}{\partial\partial ww_{ss_{jj}}} = 0, \quad \frac{\partial\partial\Pi}{\partial\partial ww_{zz_{jj}}} = 0 \tag{20bb}$$

The equations of motion can be expressed for the developed FEM model by:

$$([KK] - CC_0[GG] - \omega\omega^2[MM])\{\Delta\} = \{FF\} \tag{21aa}$$

$$\left(\begin{bmatrix} [KK_{11}] & [KK_{12}] & [KK_{13}] & [KK_{14}] \\ [KK_{12}]^{CC} & [KK_{22}] & [KK_{23}] & [KK_{24}] \\ [KK_{13}]^{CC} & [KK_{23}]^{CC} & [KK_{33}] & [KK_{34}] \\ [KK_{14}]^{CC} & [KK_{24}]^{CC} & [KK_{34}]^{CC} & [KK_{44}] \end{bmatrix} - CC_0 \begin{bmatrix} [0] & [0] & [0] & [0] \\ [0]^{CC} & [GG_{22}] & [GG_{23}] & [0] \\ [0]^{CC} & [GG_{23}]^{CC} & [GG_{33}] & [0] \\ [0]^{CC} & [0]^{CC} & [0]^{CC} & [0] \end{bmatrix} - \omega\omega^2 \begin{bmatrix} [MM_{11}] & [MM_{12}] & [MM_{13}] & [0] \\ [MM_{12}]^{CC} & [MM_{22}] & [MM_{23}] & [MM_{24}] \\ [MM_{13}]^{CC} & [MM_{23}]^{CC} & [MM_{33}] & [MM_{34}] \\ [MM_{14}]^{CC} & [MM_{24}]^{CC} & [MM_{34}]^{CC} & [MM_{44}] \end{bmatrix}\right) \begin{Bmatrix} uu_{jj} \\ ww_{bb_{jj}} \\ ww_{ss_{jj}} \\ ww_{zz_{jj}} \end{Bmatrix} = \begin{Bmatrix} \{0\} \\ \{FF_2\} \\ \{FF_3\} \\ \{FF_4\} \end{Bmatrix} \tag{21bb}$$

where $[KK_{kkkk}]$, $[GG_{kkkk}]$ and $[MM_{kkkk}]$ are the stiffness, geometric stiffness and mass matrices, respectively. The nodal force vector is FF_{kk}. The mechanical behaviours of the CNTRC and GPLRC beams can be obtained in terms of displacements, frequencies and buckling loads by using developed FEM model in Eq. (21). The boundary conditions (BC) can be given by:

Simply Supported (S):

$$uu = ww_{bb} = ww_{ss} = ww_{zz} = 0 \; aatt \; xx = 0 \; aaaadd \; xx = aa$$

Clamped (C):

$$uu = ww_{bb} = ww_{bb,xx} = ww_{ss} = ww_{ss,xx} = ww_{zz} = ww_{zz,xx} = 0 \; aatt \; xx = 0 \; aaaadd \; xx = aa$$

3. Numerical Results

The structural behaviors of CNTRC and GPLRC beams, whose material properties are provided in Table 1, are investigated by using a SNDT and FEM with respect to various BCs. It should be noted that CC_{GG} is set to 10 for GPLRC beams. For convenience, the transverse displacements, bifurcation buckling loads and natural frequencies are expressed by using following dimensionless formulas:

DCD $\bar{w} = w\left(\frac{GG}{2}\right) \frac{100 EE_{mm} h^3}{qq_{GG}^4}$: dimensionless central deflection

DCBL $\bar{C}_{cccc} = C_0 \frac{GG^2}{EE_{mm} h^3}$: dimensionless critical buckling loads

DFF $(\Omega = \frac{\omega \rho_{mm}(1-\nu_{mm}^2)}{EE_{mm}})$: dimensionless natural frequency

Table 1 About Here

3.1. Convergence study

The developed FEM model based on a SNDT is evaluated and verified by performing several convergence and comparison studies. In Table 2, a convergence study for the DCBLs of S-S CNTRC beams based on the various CNT patterns, namely, UD, O, X and V, is carried by employing various number of elements (20, 30, 40 and 50) which are distributed uniformly through the length of the beam. The results are compared with those given by Wattanasakulpong and Ungbhakorn [29], who used Third-order Beam Theory (TBT) and a good agreement is seen. It should be noted that the effect of the number of elements employed in the presented FEM model is not observed in this case.

Table 2 About Here

Second convergence study is carried out by employing X-GPLRC beams for the computation of DCBLs with respect to various BCs and aspect ratios in Table 3. Again, for the S-S and C-S GPLRC beams, the effect of employing different number of elements on the DCBL are not observed. Comparisons performed with the study [21], who used First-order Beam Theory (FBT), indicate that a very good agreement is detected between the numerical results for both cases. The convergence and comparison studies indicate that the presented FEM model with 40 elements can yield satisfactory results.

3.2. Results for bending analysis

Tables 4 and 5 show the deflections for various types of CNTRC and GPLRC beams subjected to a uniform load with different CNT volume fraction VV^*_{CCCCC}, GPL weight fractions WW_{GGGGGG}, distribution patterns, and slenderness ratios L/h. The obtained results for UD-CNTRC S-S beams are compared with those reported by Wattanasakulpong and Ungbhakorn [29] based on TBT. An excellent agreement between the results is found for all cases. The effects of VV^*_{CCCCC}, WW_{GGGGGG} and distribution of CNT and GPL on deflections of beams under a uniform load are shown in Fig. 4. It can be seen that an increase in VV^*_{CCCCC} and WW_{GGGGGG} leads to a reduction of deflection of the beam. This is due to the fact that increasing the volume fraction of CNTs and weight fractions of GPL makes the CNTRC/ GPLRC beams stiffer, and consequently, leads to a reduction of the deflection. The distribution of CNT/GPL reinforcements has significant effects on the stiffness of CNTRC/GPLRC beams. The deflections of O-beam are greatest and those of X-beam are smallest for the same amount of VV^*_{CCCCC} or WW_{GGGGGG}. This means that the distribution of CNT/GPL reinforcements is close to the top and bottom are more efficient than that nearby the mid-plane. Effects of aspect ratio (aa_{GGGGGG}/bb_{GGGGGG}) and width-to-thickness ratio (bb_{GGGGGG}/tt_{GGGGGG}), on the deflections of GPLRC beams are plotted in Fig. 5. As aa_{GGGGGG}/bb_{GGGGGG} and bb_{GGGGGG}/tt_{GGGGGG} increase, they decrease and become to be constant when bb_{GGGGGG}/tt_{GGGGGG} reaches to 10^4. It implies that GPLRC

beams that have a larger surface area and less monolayer graphene exhibit better performance than others do.

3.3. Results for free vibration and buckling analysis

Tables 6-8 show the comparison of the lowest three dimensionless frequency and the critical buckling loads of CNTRC and GPLRC C-C beams under an axial compression. The results are compared with those reported by Yas and Samadi [24] and Wu et al. [18] for natural frequencies and Wattanasakulpong and Mao [27] and Yang el al. [21] for the critical buckling loads. It should be noted that all the results from previous studies [18, 21, 24, 27] used FBT. It is reason why current results are slightly different for thick beams $(L/h = 5,10)$. It can be seen that the natural frequencies and buckling load increases with the increase of volume fraction of CNTs for CNTRC beams or GPL weight fractions for GPLRC ones. Similar to the observations in static analysis, pattern X gives the highest natural frequencies/buckling loads, followed by patterns U/UD, A, and O/V (Tables 9-11). The natural frequencies and buckling load also increases with the increase of aa_{GGGGGG}/bb_{GGGGGG} and bb_{GGGGGG}/tt_{GGGGGG} (Fig. 6). These effects become less pronounced when $bb_{GGGGGG}/tt_{GGGGGG} > 10^4$, which is the same observation with deflections. New results for both CNTRC and GPLRC beams for various configurations given in Tables 4 and 5, 10-12 can be used for reference as benchmark for future studies.

Finally, the vibration analysis of loaded CNTRC/ GPLRC beams is investigated. Verification results of the first three natural frequencies of GPLRC C-C beams under an axial compression, which are given in Table 8, show very good agreement with previous one [18]. The fundamental frequencies of CNTRC/ GPLRC beams for three cases of loads: tension ($CC_0/CC_{cccc} = -0.5$), no axial and compression ($CC_0/CC_{cccc} = 0.5$)are given in Tables 12 and 13. Figs. 7 and 8 show the relationship between fundamental frequency and axial compressive load. The smallest and largest curves correspond to O-beams and X-beams. As axial force increases, the natural

frequencies decrease and vanish at zero when $CC_0 = CC_{cccc}$. It confirms again that the tension force has a stiffening effect while the compressive force has a softening effect on the natural frequencies. They increase again when the applied axial compressive load exceeds CC_{cccc}. Vibration mode shapes of X-CNTRC and X- GPLRC C-C beams with three cases of axial load are plotted in Fig. 9. There is negligible difference between mode shapes in each case. It can be seen that the shear component is more pronounced for X- GPLRC than X-CNTRC beams.

4. Conclusions

Finite elements solutions to the bending, buckling and free vibration analyses of CNTRC/GPLRC beams are presented using a normal and shear deformation beam theory. The numerical results show that increasing the volume fraction of CNTs, GPL weight fraction will increase the stiffness of CNTRC/GPLRC beams, and consequently, leads to a reduction of deflections and an increase in buckling loads and natural frequencies. Due to increase in beams' stiffness, the distribution of CNT/GPL reinforcements is close to the top and bottom are more efficient than that nearby the mid-plane. This theory is capable of predicting accurately the responses of thin to thick beams.

Reference

[1] Thostenson ET, Ren Z, Chou TW. Advances in the science and technology of carbon nanotubes and their composites: a review. Composites Science and Technology 2001;61(13):1899-1912.

[2] Fiedler B, Gojny FH, Wichmann MHG, Nolte MCM, Schulte K. Fundamental aspects of nano-reinforced composites. Composites Science and Technology 2006;66(16):3115-3125.

[3] Esawi AMK, Farag MM. Carbon nanotube reinforced composites: Potential and current challenges. Materials & Design 2007;28(9):2394-2401.

[4] Qian D, Dickey EC, Andrews R, Rantell T. Load transfer and deformation mechanisms in carbon nanotube-polystyrene composites. Applied Physics Letters 2000;76(20):2868-2870.

[5] Wagner HD, Lourie O, Feldman Y, Tenne R. Stress-induced fragmentation of multiwall carbon nanotubes in a polymer matrix. Applied Physics Letters 1998;72(2):188-190.

[6] Liu YJ, Chen XL. Evaluations of the effective material properties of carbon nanotube-based composites using a nanoscale representative volume element. Mechanics of Materials 2003;35(1):69-81.

[7] Frankland SJV, Harik VM, Odegard GM, Brenner DW, Gates TS. The stress–strain behavior of polymer–nanotube composites from molecular dynamics simulation. Composites Science and Technology 2003;63(11):1655-1661.

[8] Han Y, Elliott J. Molecular dynamics simulations of the elastic properties of polymer/carbon nanotube composites. Computational Materials Science 2007;39(2):315-323.

[9] Seidel GD, Lagoudas DC. Micromechanical analysis of the effective elastic properties of carbon nanotube reinforced composites. Mechanics of materials 2006;38(8–10):884-907.

[10] Shen HS. Nonlinear bending of functionally graded carbon nanotube-reinforced composite plates in thermal environments. Composite Structures 2009;91(1):9-19.

[11] Song M, Kitipornchai S, Yang J. Free and forced vibrations of functionally graded polymer composite plates reinforced with graphene nanoplatelets. Composite Structures 2017;159:579–88.

[12] Liew K; Lei Z & Zhang L. Mechanical analysis of functionally graded carbon nanotube reinforced composites: A review. Composite Structures, 2015, 120, 90 - 97

[13] Zhao S, Zhao Z; Yang Z; Ke L; Kitipornchai S & Yang J. Functionally graded graphene reinforced composite structures: A review. Engineering Structures, 2020, 210, 110339

[14] Rafiee M; Yang J & Kitipornchai S. Thermal bifurcation buckling of piezoelectric carbon nanotube reinforced composite beams. Computers & Mathematics with Applications, 2013, 66, 1147 - 1160

[15] Rafiee M; Yang J. & Kitipornchai S. Large amplitude vibration of carbon nanotube reinforced functionally graded composite beams with piezoelectric layers Composite Structures, 2013, 96, 716 – 725

[16] Ke LL, Yang J, Kitipornchai S. Nonlinear free vibration of functionally graded carbon nanotube-reinforced composite beams. Composite Structures 2010;92(3):676-683.

[17] Ke LL, Yang J and Kitipornchai, S. Dynamic Stability of Functionally Graded Carbon Nanotube-Reinforced Composite Beams. Mechanics of Advanced Materials and Structures, 2013, 20, 28-37

[18] Wu H; Yang J & Kitipornchai S. Nonlinear vibration of functionally graded carbon nanotube-reinforced composite beams with geometric imperfections. Composites Part B: Engineering, 2016, 90, 86 - 96

[19] Wu H.; Kitipornchai S. & Yang J. Free Vibration and Buckling Analysis of Sandwich Beams with Functionally Graded Carbon Nanotube-Reinforced Composite Face Sheets. International Journal of Structural Stability and Dynamics, 2015, 15, 1540011

[20] Feng C, Kitipornchai S, Yang J. Nonlinear bending of polymer nanocomposite beams reinforced with non-uniformly distributed graphene platelets (GPLs). Composites Part B: Engineering 2017;110:132–40.

[21] Yang J, Wu H, Kitipornchai S. Buckling and postbuckling of functionally graded multilayer graphene platelet-reinforced composite beams. Composite Structures 161 (2017), 111-118

[22] Kitipornchai S, Chen D, Yang J. Free vibration and elastic buckling of functionally graded porous beams reinforced by graphene platelets. Material Design, 116 (2017), pp. 656-665

[23] Song M, Gong Y, Yang J, Zhu W, Kitipornchai S. Free vibration and buckling analyses of edge-cracked functionally graded multilayer graphene nanoplatelet-reinforced composite beams resting on an elastic foundation. Journal of Sound and Vibration, 458 (2019), pp. 89-108

[24] Yas MH, Samadi N. Free vibrations and buckling analysis of carbon nanotube-reinforced composite Timoshenko beams on elastic foundation. International Journal of Pressure Vessels and Piping 2012;98(10):119-128.

[25] Yas MH, Heshmati, M. Dynamic analysis of functionally graded nanocomposite beams reinforced by randomly oriented carbon nanotube under the action of moving load. Applied Mathematical Modelling, 2012, 36, 1371 - 1394

[26] Heshmati, M, Yas MH & Daneshmand, F. A comprehensive study on the vibrational behavior of CNT-reinforced composite beams. Composite Structures, 2015, 125, 434 - 448

[27] Wattanasakulpong N, Mao Q. Stability and vibration analyses of carbon nanotube-reinforced composite beams with elastic boundary conditions: Chebyshev collocation method. Mechanics of Advanced Materials and Structures 2017; 24: 260-270

[28] Ansari R, Faghih Shojaei M, Mohammadi V, Gholami R & Sadeghi F. Nonlinear forced vibration analysis of functionally graded carbon nanotube-reinforced composite Timoshenko beams. Composite Structures, 2014, 113, 316 - 327

[29] Wattanasakulpong N, Ungbhakorn V. Analytical solutions for bending, buckling and vibration responses of carbon nanotube-reinforced composite beams resting on elastic foundation. Computational Materials Science 2013;71:201-208.

[30] Lin F & Xiang Y. Vibration of carbon nanotube reinforced composite beams based on the first and third order beam theories. Applied Mathematical Modelling, 2014, 38, 3741 - 3754

[31] Shen HS, Lin F, Xiang Y. Nonlinear bending and thermal postbuckling of functionally graded graphene-reinforced composite laminated beams resting on elastic foundations Engineering Structures, 140 (2017), pp. 89-97

[32] Anirudh B, Ganapathi M, Anant C, Polit O. A comprehensive analysis of porous graphene-reinforced curved beams by finite element approach using higher-order structural theory: Bending, vibration and buckling. Composite Structures 222 (2019), p. 110899

[33] Barati MR, Zenkour AM. Post-buckling analysis of refined shear deformable graphene platelet reinforced beams with porosities and geometrical imperfection. Composite Structures, 181 (2017), pp. 194-202

[34] Koiter WT, A consistent first approximation in the general theory of thin elastic shells. in: Proceedings of first symposium on the theory of thin elastic shells, north-holland, Amsterdam

[35] Carrera E, Theories and finite elements for multilayered plates and shells: a unified compact formulation with numerical assessment and benchmarking, Archives of Computational Methods in Engineering 10 (3) (2003) 215-296.

[36] Carrera E, Brischetto S, Cinefra M, Soave M. Effects of thickness stretching in functionally graded plates and shells, Composites Part B: Engineering 42 (2) (2011) 123-133.

[37] Shen H. Thermal buckling and postbuckling behavior of functionally graded carbon nanotube-reinforced composite cylindrical shells. Composites Part B: Engineering. 2012;43(3):1030-1038. doi:10.1016/j.compositesb.2011.10.004

[38] Karamanlı A, Vo TP. Size dependent bending analysis of two directional functionally graded microbeams via a quasi-3D theory and finite element method, Composites Part B: Engineering. 144 (2018) 171-183. doi:10.1016/j.compositesb.2018.02.030.

[39] Karamanli A, Aydogdu M. Size dependent flapwise vibration analysis of rotating two-directional functionally graded sandwich porous microbeams based on a transverse shear and normal deformation theory, International Journal Of Mechanical Sciences. 159 (2019) 165-181. doi:10.1016/j.ijmecsci.2019.05.047.

[40] Karamanli A, Aydogdu M. Structural dynamics and stability analysis of 2D-FG microbeams with two-directional porosity distribution and variable material length scale parameter, Mechanics Based Design Of Structures And Machines. 48 (2019) 164-191. doi:10.1080/15397734.2019.1627219.

[41] Vo TP, Thai HT, Nguyen TK, Inam F, Lee J. Static behaviour of functionally graded sandwich beams using a quasi-3D theory. Composistes Part B 2015;68:59-74.

Table 1. Material and dimensional properties of CNTRC and GPLRC beams

CNTRC [24]	$MMaattNNNNxx$: $EE_{mm} = 2.5\ GGGGaa;\ vv_{mm} = 0.3;\ \rho\rho_{mm} = 1190\ kkkk/mm^3$ $CCCCCC$: $EE_{11}^{CCCCCC} = 600\ GGGGaa;\ EE_{22}^{CCCCCC} = 10\ GGGGaa;\ GG_{12}^{CCCCCC} = 17.2\ GGGGaa$ $GG_{12} = GG_{13};\ GG_{23} = GG_{12};\ vv_{12}^{CCCCCC} = 0.19;\ \rho\rho_{CCCCCC} = 1400\ kkkk/mm^3$
GPLRC [21]	$MMaattNNNNxx$: $EE_{mm} = 3\ GGGGaa;\ vv_{mm} = 0.34;\ \rho\rho_{mm} = 1200\ kkkk/mm^3$ $GGGGGG$: $EE_{GGGGGG} = 1.01\ CCGGaa;\ vv_{GGGGGG} = 0.186;\ \rho\rho_{GGGGGG} = 1062.5\ kkkk/mm^3$ $aa_{GGGGGG} = 2.5\mu\mu mm = 2.5xx10^{-6}mm;\ bb_{GGGGGG} = 1.5\mu\mu mm = 1.5xx10^{-6}mm$ $tt_{GGGGGG} = 1.5aamm = 1.5xx10^{-9}mm$

Table 2. Convergence studies on the DCBLs and DFFs of S-S CNTRC beams for various distribution patterns ($GG/h = 15, VV^{*}_{CCCCC} = 0.12$).

Elements	Critical buckling loads				Fundamental frequencies			
	UD-CNTRC	O-CNTRC	X-CNTRC	V-CNTRC	UD-CNTRC	O-CNTRC	X-CNTRC	V-CNTRC
20	0.0984	0.0576	0.1289	0.0923	0.9745	0.7452	1.1152	0.9441
30	0.0984	0.0576	0.1289	0.0923	0.9745	0.7452	1.1152	0.9441
40	0.0984	0.0576	0.1289	0.0923	0.9745	0.7452	1.1152	0.9441
50	0.0984	0.0576	0.1289	0.0923	0.9745	0.7452	1.1152	0.9441
TBT [29]	0.0984	0.0576	0.1289	-	0.9745	0.7453	1.1152	0.8441

Table 3. Convergence studies on the DCBLs of X-GPLRC Beam for various BCs and slenderness ratios ($CC_{GG} = 10, CC_{CCCC} = CC_0/(EE_{mm}h)$)

BC	Elements	L/h 10	20	30	40
SS	10	0.0196	0.0050	0.0023	0.0013
	20	0.0196	0.0050	0.0023	0.0013
	30	0.0196	0.0050	0.0023	0.0013
	40	0.0196	0.0050	0.0023	0.0013
	FBT [21]	0.0196	0.0050	0.0023	0.0013
CS	10	0.0387	0.0103	0.0046	0.0026
	20	0.0386	0.0102	0.0046	0.0026
	30	0.0386	0.0102	0.0046	0.0026
	40	0.0386	0.0102	0.0046	0.0026
	FBT [21]	0.0384	0.0102	0.0046	0.0026
CC	10	0.0710	0.0198	0.0090	0.0051
	20	0.0706	0.0197	0.0089	0.0051
	30	0.0705	0.0197	0.0089	0.0051
	40	0.0704	0.0196	0.0089	0.0051
	50	0.0704	0.0196	0.0089	0.0051
	FBT [21]	0.0709	0.0196	0.0089	0.0050

Table 4. DCDs of CNTRC beams with different volume fraction, distribution patterns, boundary conditions and slenderness ratios

Beam	VV^{*}_{CCCCCC}	Reference	S-S			C-C			C-S			C-F		
			$GG/h = 5$	10	15	5	10	15	5	10	15	5	10	15
UD-CNTRC	0.12	TBT [29]	-	0.7040	0.5240	-	-	-	-	-	-	-	-	-
		Present (TBT)	1.6445	0.7038	0.5240	1.0433	0.3605	0.2087	1.2576	0.4556	0.2904	4.4356	2.1855	1.6998
		Present	1.6443	0.7038	0.5240	1.0439	0.3606	0.2087	1.2579	0.4557	0.2904	4.5351	2.1856	1.6999
O-CNTRC		Present	2.1637	1.0977	0.8978	1.3549	0.4792	0.2993	1.6071	0.6407	0.4510	6.3683	3.5317	2.9710
X-CNTRC		Present	1.4964	0.5767	0.3995	0.9674	0.3277	0.1811	1.1678	0.4001	0.2389	3.9989	1.7478	1.2747
V-CNTRC		Present	1.8177	0.8785	0.6990	1.0784	0.3953	0.2435	1.3269	0.5253	0.3603	5.1274	2.7802	2.2952
UD-CNTRC	0.17	TBT [29]	-	0.4490	0.3440	-	-	-	-	-	-	-	-	-
		Present (TBT)	1.0023	0.4490	0.3438	0.6322	0.2201	0.1300	0.7602	0.2824	0.1850	2.8071	1.4085	1.1220
		Present	1.0022	0.4490	0.3438	0.6327	0.2201	0.1300	0.7604	0.2824	0.1850	2.8081	1.4086	1.1221
O-CNTRC		Present	1.3210	0.7128	0.5990	0.8020	0.2919	0.1884	0.9578	0.4006	0.2921	3.9497	2.3124	1.9912
X-CNTRC		Present	0.9178	0.3661	0.2603	0.5956	0.2015	0.1129	0.7150	0.2484	0.1515	2.4877	1.1206	0.8362
V-CNTRC		Present	1.1221	0.5711	0.4663	0.6557	0.2441	0.1543	0.8074	0.3309	0.2339	3.2193	1.8243	1.5389
UD-CNTRC	0.28	TBT [29]	-	0.3250	0.2350	-	-	-	-	-	-	-	-	-
		Present (TBT)	0.7952	0.3250	0.2346	0.5050	0.1739	0.0987	0.6116	0.2167	0.1343	2.1547	0.9977	0.7556
		Present	0.7951	0.3250	0.2346	0.5052	0.1739	0.0987	0.6117	0.2167	0.1343	2.1554	0.9977	0.7557
O-CNTRC		Present	0.9569	0.4798	0.3903	0.6039	0.2121	0.1316	0.7146	0.2821	0.1972	2.8109	1.5414	1.2905
X-CNTRC		Present	0.7667	0.2806	0.1860	0.4889	0.1670	0.0906	0.5974	0.2014	0.1163	1.9998	0.8355	0.5861
V-CNTRC		Present	0.8630	0.4005	0.3117	0.5151	0.1874	0.1133	0.6352	0.2456	0.1644	2.3983	1.2567	1.0184

Table 5. DCDs of GPLRC beams with different GPL weight fractions, distribution patterns, boundary conditions and slenderness ratios ($\mathcal{C}_{\mathcal{G}\mathcal{G}} = 10$).

BC	WW_{GGGGGG}	$\mathcal{G}\mathcal{G}/h = 5$				$\mathcal{G}\mathcal{G}/h = 10$				$\mathcal{G}\mathcal{G}/h = 20$			
		U-GPLRC	X-GPLRC	O-GPLRC	A-GPLRC	U-GPLRC	X-GPLRC	O-GPLRC	A-GPLRC	U-GPLRC	X-GPLRC	O-GPLRC	A-GPLRC
SS	0.1 %	12.8174	11.6755	14.3164	13.0320	12.0026	10.7768	13.5732	12.2173	11.7981	10.5513	13.3866	12.0128
	0.3 %	8.5528	7.2042	10.8989	9.1649	8.0092	6.5370	10.4452	8.6215	7.8728	6.3696	10.3312	8.4851
	0.5 %	6.4175	5.2257	8.8203	7.1735	6.0097	4.6954	8.4948	6.7659	5.9073	4.5624	8.4130	6.6636
CS	0.1 %	5.7562	5.3587	6.3071	5.8314	4.9448	4.4720	5.5576	5.0200	4.7430	4.2501	5.3726	4.8181
	0.3 %	3.8410	3.3896	4.7202	4.0541	3.2996	2.7362	4.2544	3.5127	3.1650	2.5719	4.1406	3.3780
	0.5 %	2.8820	2.4928	3.7902	3.1439	2.4759	1.9753	3.4519	2.7377	2.3748	1.8448	3.3697	2.6365
CC	0.1 %	3.4149	3.2592	3.6564	3.4578	2.6049	2.3808	2.9012	2.6478	2.4005	2.1578	2.7120	2.4434
	0.3 %	2.2787	2.1179	2.6784	2.4009	1.7382	1.4749	2.2034	1.8606	1.6019	1.3107	2.0854	1.7243
	0.5 %	1.7097	1.5800	2.1291	1.8607	1.3043	1.0722	1.7814	1.4555	1.2020	0.9423	1.6955	1.3532
CF	0.1 %	42.6311	38.7168	47.7446	43.3609	40.3942	36.2446	45.7061	41.1242	39.8733	35.6544	45.2471	40.6033
	0.3 %	28.4479	23.8074	36.4404	30.5293	26.9551	21.9680	35.1926	29.0370	26.6075	21.5204	34.9243	28.6895
	0.5 %	21.3461	17.2355	29.5292	23.9171	20.2259	15.7722	28.6297	22.7975	19.9650	15.4132	28.4418	22.5367

Table 6. Comparisons for the first three natural frequencies of CNTRC beams with different volume fraction, distribution patterns, and boundary conditions ($\mathbb{G}/h = 15$)

Beams	VV^{*}_{CCCCCC}	Reference	C-C			C-S			S-S			C-F		
			$\omega\omega_1$	$\omega\omega_2$	$\omega\omega_3$	$\omega\omega_1$	$\omega\omega_2$	$\omega\omega_3$	$\omega\omega_1$	$\omega\omega_2$	$\omega\omega_3$	$\omega\omega_1$	$\omega\omega_2$	$\omega\omega_3$
UD-CNTRC	0.12	FBT [24]	1.5085	3.1353	4.9979	1.2444	3.0159	4.9342	0.9753	2.8728	4.8704	0.3764	1.7006	3.6648
		Present	1.5489	3.4106	5.3095	1.3025	3.1219	5.1310	0.9745	2.8801	4.9291	0.3772	1.7328	3.7746
X-CNTRC		FBT [24]	1.6000	3.2629	5.1514	1.3577	3.1817	5.1092	1.1150	3.0814	5.0695	0.4416	1.8497	3.8777
		Present	1.6591	3.5809	5.5468	1.4361	3.3160	5.3652	1.1152	3.1010	5.1691	0.4434	1.8996	4.0280
O-CNTRC		FBT [24]	1.3180	2.8762	4.6840	1.0331	2.6814	4.5619	0.7527	2.4562	4.4320	0.2809	1.4266	3.2489
		Present	1.2976	2.9572	4.6444	1.0448	2.6584	4.4865	0.7452	2.3961	4.2901	0.2797	1.4073	3.1952
V-CNTRC		FBT [24]	1.4068	2.9997	4.8363	1.1529	2.8472	4.7474	0.9453	2.6424	4.6675	0.3193	1.5473	3.4380
		Present	1.4370	3.2472	5.1195	1.1891	2.9425	4.9218	0.9441	2.6451	4.7113	0.3197	1.5696	3.5286
UD-CNTRC	0.17	FBT [24]	1.9144	4.0187	6.4348	1.5602	3.8402	6.3370	1.1999	3.6276	6.2363	0.4587	2.1365	4.6614
		Present	1.9556	4.3453	6.7802	1.6246	3.9580	6.5507	1.1983	3.6291	6.2851	0.4594	2.1681	4.7769
X-CNTRC		FBT [24]	2.0498	4.2111	6.6753	1.7188	4.0843	6.6094	1.3830	3.9293	6.5447	0.5413	2.3437	4.9706
		Present	2.0938	4.5469	7.0464	1.7955	4.1963	6.8200	1.3760	3.9095	6.5703	0.5416	2.3778	5.0870
O-CNTRC		FBT [24]	1.6500	3.6565	5.9970	1.2769	3.3772	5.8126	0.9155	3.0577	5.6139	0.3394	1.7685	4.0913
		Present	1.6305	3.7681	5.9610	1.2924	3.3617	5.7418	0.9087	2.9988	5.4663	0.3384	1.7502	4.0383
V-CNTRC		FBT [24]	1.7721	3.8312	6.2139	1.4344	3.6064	6.0765	1.1609	3.3084	5.9498	0.3866	1.9287	4.3500
		Present	1.7994	4.1115	6.5107	1.4715	3.7049	6.2516	1.1583	3.3024	5.9728	0.3868	1.9476	4.4360
UD-CNTRC	0.28	FBT [24]	2.1618	4.4556	7.0745	1.8040	4.3112	6.9987	1.4401	4.1362	6.9245	0.5612	2.4614	5.2446
		Present	2.2195	4.8445	7.5304	1.8895	4.4557	7.2754	1.4361	4.1341	6.9942	0.5621	2.5072	5.3990
X-CNTRC		FBT [24]	2.3169	4.7051	7.4093	1.9813	4.6030	7.3560	1.6493	4.4752	7.3068	0.6586	2.6987	5.6150
		Present	2.3121	4.9467	7.6652	2.0298	4.6028	7.4020	1.6113	4.3253	7.1269	0.6528	2.6840	5.6111
O-CNTRC		FBT [24]	1.9284	4.1740	6.7728	1.5229	3.9112	6.6127	1.1202	3.6056	6.4434	0.4197	2.0993	4.7399
		Present	1.9296	4.3857	6.8776	1.5586	3.9486	6.6486	1.1149	3.5665	6.3639	0.4191	2.0970	4.7466
V-CNTRC		FBT [24]	2.0504	4.3414	6.9783	1.6933	4.1393	6.8633	1.4027	3.8639	6.7618	0.4761	2.2685	5.0007
		Present	2.0766	4.6536	7.3184	1.7357	4.2353	7.0384	1.3930	3.8299	6.7447	0.4757	2.2854	5.0860

Table 7. Comparisons for DCBLs of CNTRC beams with different volume fraction, distribution patterns, boundary conditions and slenderness ratios

Beams	VV^{*}_{CCCCCC}	Reference	C-C			C-S			S-S			C-F		
			$GG/h = 5$	10	15	5	10	15	5	10	15	5	10	15
UD- CNTRC	0.12	FBT [24]	0.3244	0.271	0.2126	0.2887	0.2115	0.1488	0.271	0.1634	0.0983	-	-	-
		Present	0.2968	0.2798	0.2151	0.2967	0.2271	0.1558	0.2798	0.1642	0.0984	0.1640	0.0631	0.0312
X- CNTRC		FBT [24]	0.3332	0.2931	0.2441	0.3042	0.239	0.1804	0.2931	0.1978	0.1283	-	-	-
		Present	0.3231	0.3075	0.2491	0.3228	0.2601	0.1914	0.3075	0.1999	0.1289	0.1996	0.0862	0.0443
O- CNTRC		FBT [24]	0.3069	0.2252	0.156	0.2586	0.1608	0.0992	0.2252	0.1091	0.0587	-	-	-
		Present	0.2725	0.2126	0.1492	0.2601	0.1604	0.0990	0.2126	0.1056	0.0576	0.1055	0.0352	0.0167
V- CNTRC		FBT [24]	0.2970	0.2535	0.1822	0.2969	0.2005	0.1293	0.2744	0.1565	0.0923	0.1318	0.0458	0.0220
UD- CNTRC	0.17	FBT [24]	0.549	0.4471	0.3414	0.4829	0.3423	0.2335	0.4471	0.2566	0.15	-	-	-
		Present	0.4894	0.4591	0.3445	0.4892	0.3656	0.2436	0.4591	0.2575	0.1502	0.2573	0.0949	0.0463
X- CNTRC		FBT [24]	0.5695	0.4911	0.3994	0.5146	0.3935	0.2886	0.4911	0.3167	0.1989	-	-	-
		Present	0.5187	0.5011	0.3994	0.5184	0.4187	0.3009	0.5011	0.3152	0.1979	0.3148	0.1303	0.0660
O- CNTRC		FBT [24]	0.5171	0.364	0.2437	0.4286	0.2535	0.1515	0.364	0.1666	0.0875	-	-	-
		Present	0.4683	0.3485	0.2358	0.4367	0.2552	0.1520	0.3485	0.1628	0.0864	0.1627	0.0522	0.0245
V- CNTRC		FBT [24]	0.4907	0.4108	0.2868	0.4905	0.3184	0.1990	0.4495	0.2445	0.1401	0.2029	0.0679	0.0322
UD- CNTRC	0.28	FBT [24]	0.6504	0.5566	0.4487	0.5854	0.4431	0.3215	0.5566	0.353	0.2193	-	-	-
		Present	0.6160	0.5788	0.4551	0.6156	0.4783	0.3384	0.5788	0.3552	0.2197	0.3549	0.1434	0.0720
X- CNTRC		FBT [24]	0.6921	0.6173	0.523	0.6366	0.51	0.3931	0.6173	0.4309	0.2867	-	-	-
		Present	0.6554	0.6005	0.4978	0.6549	0.5172	0.3949	0.6005	0.4104	0.2764	0.4098	0.1902	0.1007
O- CNTRC		FBT [24]	0.6424	0.4838	0.3427	0.5468	0.351	0.2214	0.4838	0.2434	0.1331	-	-	-
		Present	0.6139	0.4807	0.3396	0.5854	0.3646	0.2266	0.4807	0.2415	0.1325	0.2414	0.0812	0.0386
V- CNTRC		FBT [24]	0.6228	0.5340	0.3922	0.6224	0.4293	0.2840	0.5749	0.3412	0.2064	0.2888	0.1039	0.0503

Table 8. Comparisons for the DCBLs and the first three natural frequencies of GPLRC C-C beams under an axial compression ($WW_{GGGGGG} = 0.3\%$, $CC_{GG} = 10$, L/h =10).

Beams	Reference	N_{cr}	$CC_0/CC_{cccc} = 0$			$CC_0/CC_{cccc} = 0.25$			$CC_0/CC_{cccc} = 0.5$		
			$\omega\omega_1$	$\omega\omega_2$	$\omega\omega_3$	$\omega\omega_1$	$\omega\omega_2$	$\omega\omega_3$	$\omega\omega_1$	$\omega\omega_2$	$\omega\omega_3$
U-GPLRC	FBT [18]	0.0586	0.8475	2.1546	3.8662	0.7386	2.0051	3.6944	0.6075	1.8421	3.5139
	Present (TBT)	0.0586	0.8488	2.2000	2.8921	0.7396	2.0505	3.7191	0.6080	1.8879	3.5375
	Present	0.0525	0.8104	2.1122	3.7650	0.7060	1.9694	3.6006	0.5804	1.8142	3.4280
X-GPLRC	FBT [18]	0.0709	0.9293	2.3325	4.1399	0.8103	2.1667	3.9464	0.6668	1.9856	3.7427
	Present (TBT)	0.0692	0.9186	2.3394	4.0405	0.8008	2.1745	3.8436	0.6590	1.9943	3.6359
	Present	0.0623	0.8793	2.2542	3.9239	0.7666	2.0968	3.7376	0.6307	1.9249	3.5410
O-GPLRC	FBT [18]	0.0458	0.7508	1.9355	3.5171	0.6540	1.8045	3.3692	0.5375	1.6621	3.2142
	Present (TBT)	0.0462	0.7557	1.9857	3.5866	0.6580	1.8544	3.4386	0.5406	1.7121	3.2838
	Present	0.0413	0.7201	1.9011	3.4581	0.6270	1.7759	3.3171	0.5151	1.6401	3.1695
A-GPLRC	FBT [18]	0.0543	0.8164	2.0835	3.7512	0.7114	1.9401	3.5876	0.5849	1.784	3.4158
	Present (TBT)	0.0544	0.8175	2.1246	3.7749	0.7122	1.9812	3.6102	0.5853	1.8252	3.4372
	Present	0.0491	0.7831	2.0453	3.6593	0.6821	1.9079	3.5021	0.5607	1.7586	3.3370

Table 9. DFFs of CNTRC beams with different volume fraction, distribution patterns, boundary conditions and slenderness ratios

Beams	V_{CCCCCC}^{*}	C-C			C-S			S-S			C-F		
		$GG/h = 5$	10	15	5	10	15	5	10	15	5	10	15
UD-CNTRC	0.12	2.0734	1.7613	1.5489	1.8769	1.5588	1.3025	1.6430	1.2582	0.9745	0.7728	0.5191	0.3772
X-CNTRC		2.1564	1.8459	1.6591	1.9489	1.6634	1.4361	1.7230	1.3890	1.1152	0.8352	0.5936	0.4434
O-CNTRC		1.8132	1.5303	1.2976	1.6579	1.3146	1.0448	1.4300	1.0082	0.7452	0.6373	0.3969	0.2797
V-CNTRC		2.0409	1.6850	1.4370	1.8354	1.4685	1.1891	1.6270	1.2290	0.9441	0.7108	0.4501	0.3197
UD-CNTRC	0.17	2.6500	2.2455	1.9556	2.4029	1.9716	1.6246	2.0950	1.5688	1.1983	0.9718	0.6383	0.4594
X-CNTRC		2.7344	2.3441	2.0938	2.4794	2.1023	1.7955	2.1901	1.7363	1.3760	1.0502	0.7324	0.5416
O-CNTRC		2.3460	1.9542	1.6305	2.1379	1.6551	1.2924	1.8221	1.2462	0.9087	0.7972	0.4841	0.3384
V-CNTRC		2.6043	2.1363	1.7994	2.3437	1.8447	1.4715	2.0729	1.5291	1.1583	0.8860	0.5489	0.3868
UD-CNTRC	0.28	2.9427	2.5009	2.2195	2.6558	2.2296	1.8895	2.3314	1.8259	1.4361	1.1122	0.7649	0.5621
X-CNTRC		2.9963	2.5507	2.3121	2.6890	2.3128	2.0298	2.3756	1.9635	1.6113	1.1710	0.8580	0.6528
O-CNTRC		2.6789	2.2683	1.9296	2.4526	1.9542	1.5586	2.1213	1.5043	1.1149	0.9484	0.5937	0.4191
V-CNTRC		2.9151	2.4131	2.0766	2.6167	2.1176	1.7357	2.3233	1.7901	1.3930	1.0312	0.6650	0.4757

Table 10. DFFs of GPLRC beams with different GPL weight fractions, distribution patterns boundary conditions and slenderness ratios

BC	WW_{GGGGGG}	$GG/h = 5$				$GG/h = 10$				$GG/h = 20$			
		U-GPLRC	X-GPLRC	O-GPLRC	A-GPLRC	U-GPLRC	X-GPLRC	O-GPLRC	A-GPLRC	U-GPLRC	X-GPLRC	O-GPLRC	A-GPLRC
SS	0.1 %	0.5816	0.6096	0.5501	0.5807	0.3042	0.3211	0.2861	0.3037	0.1540	0.1628	0.1446	0.1537
	0.3 %	0.7120	0.7764	0.6304	0.7073	0.3725	0.4123	0.3262	0.3698	0.1885	0.2096	0.1646	0.1872
	0.5 %	0.8221	0.9119	0.7008	0.8131	0.4301	0.4865	0.3617	0.4251	0.2177	0.2477	0.1824	0.2151
CS	0.1 %	0.8624	0.8950	0.8230	0.8566	0.4688	0.4931	0.4421	0.4653	0.2400	0.2535	0.2255	0.2381
	0.3 %	1.0559	1.1269	0.9504	1.0268	0.5740	0.6306	0.5053	0.5563	0.2938	0.3260	0.2569	0.2845
	0.5 %	1.2192	1.3151	1.0602	1.1654	0.6627	0.7424	0.5610	0.6303	0.3392	0.3849	0.2848	0.3222
CC	0.1 %	1.1456	1.1726	1.1071	1.1383	0.6619	0.6922	0.6273	0.6565	0.3460	0.3649	0.3256	0.3430
	0.3 %	1.4026	1.4546	1.2935	1.3654	0.8104	0.8793	0.7201	0.7831	0.4237	0.4682	0.3714	0.4083
	0.5 %	1.6195	1.6841	1.4508	1.5504	0.9357	1.0312	0.8010	0.8854	0.4891	0.5523	0.4119	0.4609
CF	0.1 %	0.2151	0.2265	0.2026	0.2132	0.1097	0.1159	0.1030	0.1087	0.0551	0.0583	0.0517	0.0546
	0.3 %	0.2633	0.2901	0.2313	0.2538	0.1343	0.1491	0.1173	0.1293	0.0674	0.0750	0.0588	0.0650
	0.5 %	0.3040	0.3418	0.2567	0.2865	0.1550	0.1761	0.1301	0.1459	0.0779	0.0887	0.0652	0.0733

Table 11. DCBLs of GPLRC beams with different GPL weight fractions and distribution patterns, boundary conditions and slenderness ratios.

$$\blacklozenge NN_{cccc} = NN\ \frac{LL^{22}}{00}$$
$$EE_{mmhh}{}^{33}\blacklozenge$$

BC	WW_{GGGGGG}	$GG/h = 5$				$GG/h = 10$				$GG/h = 20$			
		U-GPLRC	X-GPLRC	O-GPLRC	A-GPLRC	U-GPLRC	X-GPLRC	O-GPLRC	A-GPLRC	U-GPLRC	X-GPLRC	O-GPLRC	A-GPLRC
SS	0.1 %	0.9848	1.0809	0.8818	0.9689	1.0656	1.1867	0.9424	1.0470	1.0879	1.2165	0.9589	1.0685
	0.3 %	1.4759	1.7514	1.1586	1.3789	1.5969	1.9561	1.2247	1.4840	1.6304	2.0150	1.2425	1.5128
	0.5 %	1.9670	2.4143	1.4317	1.7630	2.1283	2.7230	1.5060	1.8914	2.1728	2.8131	1.5258	1.9265
CS	0.1 %	1.8312	1.9760	1.6646	1.8083	2.1259	2.3546	1.8889	2.0952	2.2141	2.4720	1.9538	2.1807
	0.3 %	2.7443	3.1402	2.2167	2.6044	3.1860	3.8559	2.4648	2.9992	3.3180	4.0875	2.5344	3.1160
	0.5 %	3.6576	4.2822	2.7565	3.3623	4.2460	5.3476	3.0363	3.8536	4.4219	5.7005	3.1137	3.9982
CC	0.1 %	3.0494	3.2132	2.8336	3.0112	3.9631	4.3485	3.5498	3.8986	4.2800	4.7659	3.7854	4.2049
	0.3 %	4.5702	4.9753	3.8513	4.3352	5.9392	7.0434	4.6648	5.5470	6.4140	7.8553	4.9197	5.9588
	0.5 %	6.0913	6.6908	4.8360	5.5922	7.9154	9.7073	5.7652	7.0902	8.5481	10.9347	6.0496	7.5931
CF	0.1 %	0.2679	0.2982	0.2370	0.2632	0.2729	0.3051	0.2405	0.2680	0.2740	0.3067	0.2413	0.2691
	0.3 %	0.4015	0.4915	0.3081	0.3729	0.4089	0.5053	0.3117	0.3793	0.4106	0.5086	0.3124	0.3808
	0.5 %	0.5350	0.6840	0.3789	0.4752	0.5450	0.7053	0.3828	0.4830	0.5472	0.7106	0.3835	0.4848

Table 12. DFFs of CNTRC beams under an axial load with different volume fraction, distribution patterns and boundary conditions ($\mathbb{G}\mathbb{G}/h = 10$)

$\blacklozenge NN_{cccc} = NN_{00}{}^{11-\nu\nu^{22}}_{EE_{mm}} \blacklozenge$

Beams	VV^{*}_{cccccc}	S-S				C-S				C-C			
		DCBL	$CC_0/CC_{cccc} = -0.5$	0	0.5	DCBL	$CC_0/CC_{cccc} = -0.5$	0	0.5	DCBL	$CC_0/CC_{cccc} = -0.5$	0	0.5
V-CNTRC	0.12	0.1565	1.5051	1.2290	0.8692	0.2005	1.7834	1.4685	1.0530	0.2535	2.0405	1.6850	1.2154
O-CNTRC		0.1056	1.2348	1.0082	0.7130	0.1604	1.5952	1.3146	0.9439	0.2126	1.8527	1.5303	1.1051
X-CNTRC		0.1999	1.7012	1.3890	0.9822	0.2601	2.0211	1.6634	1.1934	0.3075	2.2374	1.8459	1.3303
UD-CNTRC		0.1642	1.5410	1.2582	0.8897	0.2271	1.8931	1.5588	1.1188	0.2798	2.1341	1.7613	1.2700
V-CNTRC	0.17	0.2445	1.8725	1.5291	1.0813	0.3184	2.2401	1.8447	1.3228	0.4108	2.5864	2.1363	1.5412
O-CNTRC		0.1628	1.5262	1.2462	0.8812	0.2552	2.0081	1.6551	1.1881	0.3485	2.3649	1.9542	1.4119
X-CNTRC		0.3152	2.1266	1.7363	1.2277	0.4187	2.5538	2.1023	1.5086	0.5011	2.8410	2.3441	1.6897
UD-CNTRC		0.2575	1.9214	1.5688	1.1094	0.3656	2.3938	1.9716	1.4152	0.4591	2.7202	2.2455	1.6197
V-CNTRC	0.28	0.3412	2.1922	1.7901	1.2660	0.4293	2.5723	2.1176	1.5184	0.5340	2.9227	2.4131	1.7400
O-CNTRC		0.2415	1.8424	1.5043	1.0637	0.3646	2.3714	1.9542	1.4033	0.4807	2.7464	2.2683	1.6380
X-CNTRC		0.4104	2.4048	1.9635	1.3884	0.5172	2.8108	2.3128	1.6587	0.6005	3.0918	2.5507	1.8377
UD-CNTRC		0.3552	2.2363	1.8259	1.2911	0.4783	2.7082	2.2296	1.5999	0.5788	3.0305	2.5009	1.8028

Table 13. DFFs of GPLRC beams an axial load with different GPL weight fractions, distribution patterns and boundary conditions ($\mathbb{GG}/h = 10$)

Beams	WW_{GGGGGG}	S-S				C-S				C-C			
		DCBL	$CC_0/CC_{cccc} = -0.5$	0	0.5	DCBL	$CC_0/CC_{cccc} = -0.5$	0	0.5	DCBL	$CC_0/CC_{cccc} = -0.5$	0	0.5
U-GPLRC	0.1 %	1.0656	0.3727	0.3042	0.2150	2.1259	0.5707	0.4688	0.3340	3.9631	0.8025	0.6619	0.4740
X- GPLRC		1.1867	0.3932	0.3211	0.2270	2.3546	0.6000	0.4931	0.3515	4.3485	0.8389	0.6922	0.4960
O- GPLRC		0.9424	0.3504	0.2861	0.2022	1.8889	0.5383	0.4421	0.3149	3.5498	0.7610	0.6273	0.4490
A- GPLRC		1.0620	0.3721	0.3037	0.2146	2.0952	0.5664	0.4653	0.3314	3.8986	0.7960	0.6565	0.4700
U-GPLRC	0.3 %	1.5969	0.4562	0.3725	0.2634	3.1860	0.6987	0.5740	0.4089	5.9392	0.9826	0.8104	0.5804
X- GPLRC		1.9561	0.5050	0.4123	0.2915	3.8559	0.7673	0.6306	0.4496	7.0434	1.0650	0.8793	0.6307
O- GPLRC		1.2247	0.3994	0.3262	0.2308	2.4648	0.6152	0.5053	0.3600	4.6648	0.8738	0.7201	0.5151
A- GPLRC		1.5743	0.4529	0.3698	0.2616	2.9992	0.6773	0.5563	0.3963	5.5470	0.9497	0.7831	0.5607
U-GPLRC	0.5 %	2.1283	0.5266	0.4301	0.3042	4.2460	0.8067	0.6627	0.4722	7.9154	1.1345	0.9357	0.6701
X- GPLRC		2.7230	0.5959	0.4865	0.3440	5.3476	0.9032	0.7424	0.5295	9.7073	1.2487	1.0312	0.7401
O- GPLRC		1.5060	0.4431	0.3617	0.2557	3.0363	0.6831	0.5610	0.3995	5.7652	0.9722	0.8010	0.5727
A- GPLRC		2.0790	0.5206	0.4251	0.3005	3.8536	0.7673	0.6303	0.4490	7.0902	1.0738	0.8854	0.6338

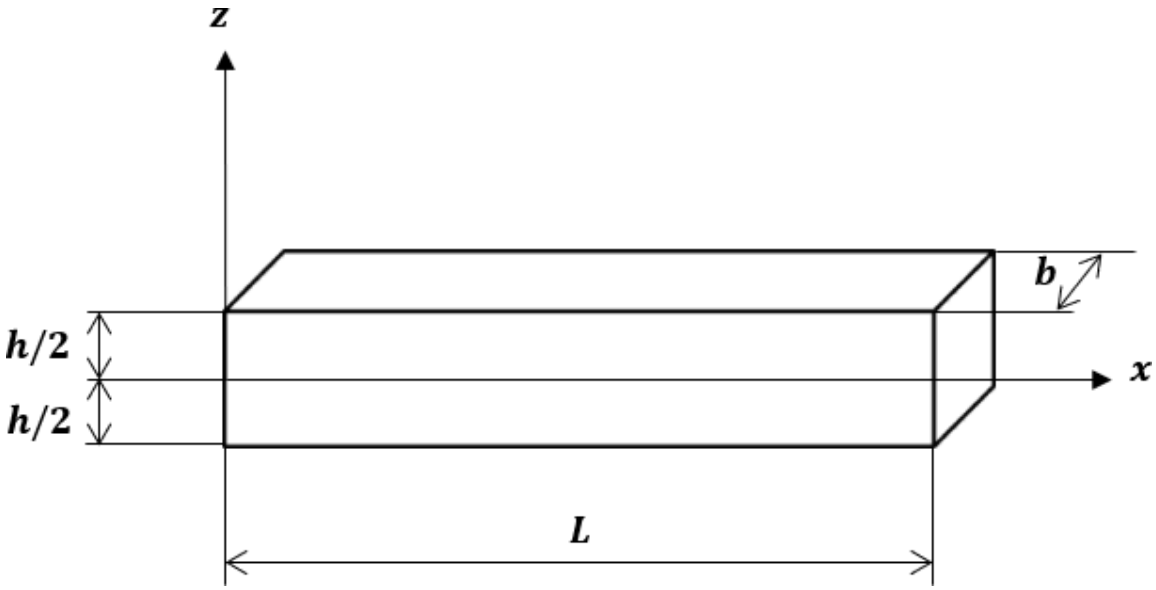

Figure 1. Geometry and co-ordinates of the studied beam

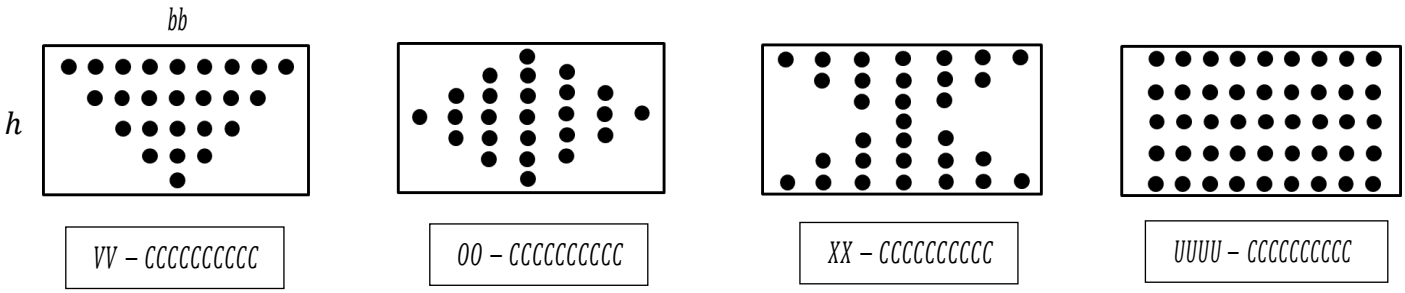

Figure 2. CNT distribution patterns

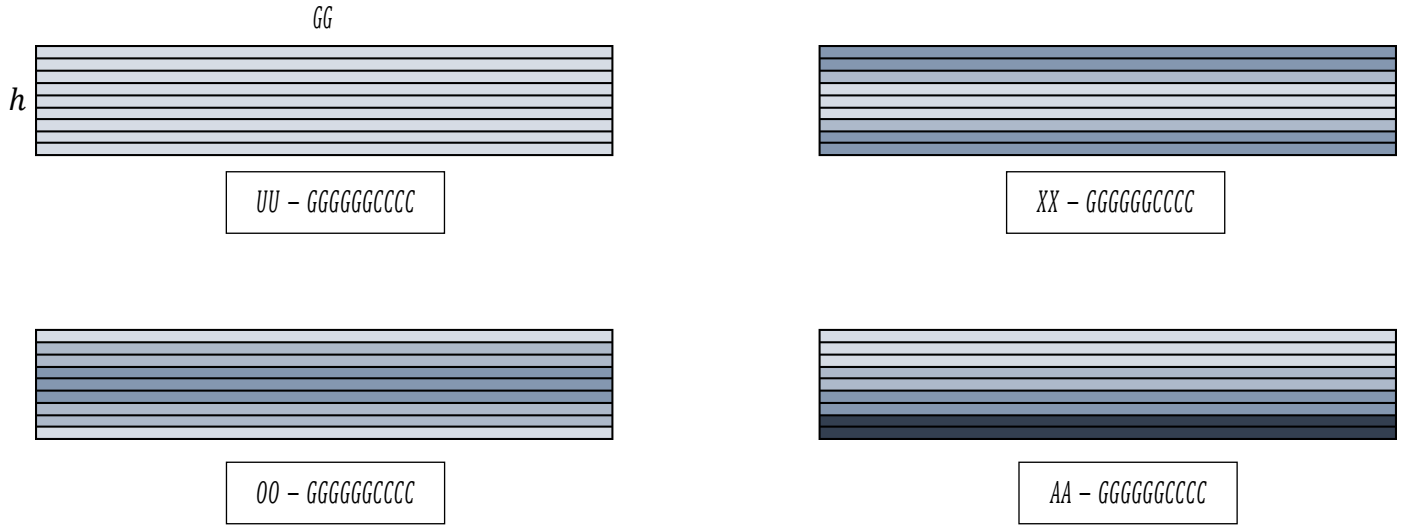

Figure 3. GPLs distribution patterns

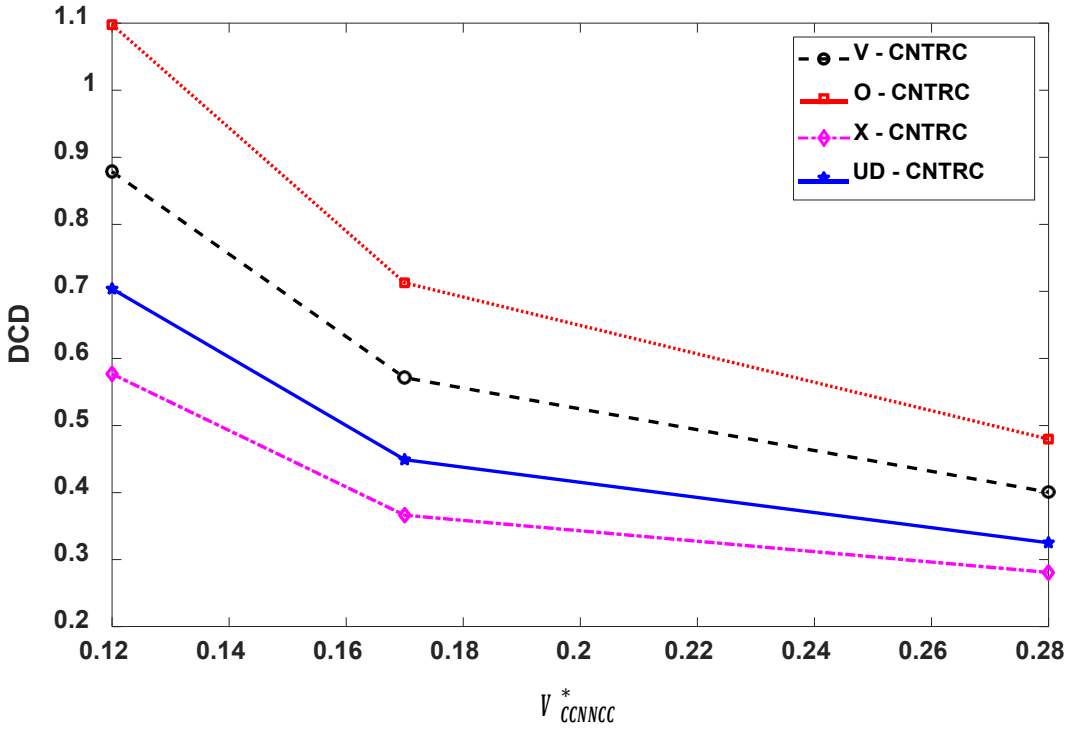

a. CNTRC beams

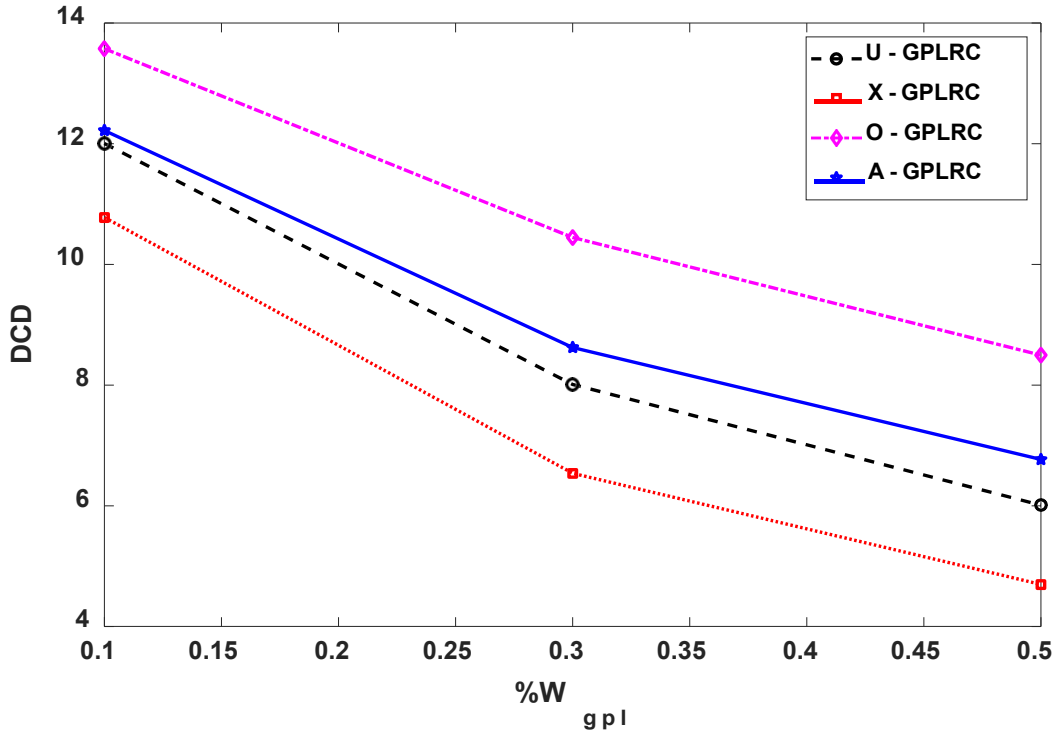

b. GPLRC beams

Figure 4. Effect of volume fraction and WW_{GGGGGG} on deflection for various CNTRC and GPLRC S-S beams ($𝔾/h = 10$)

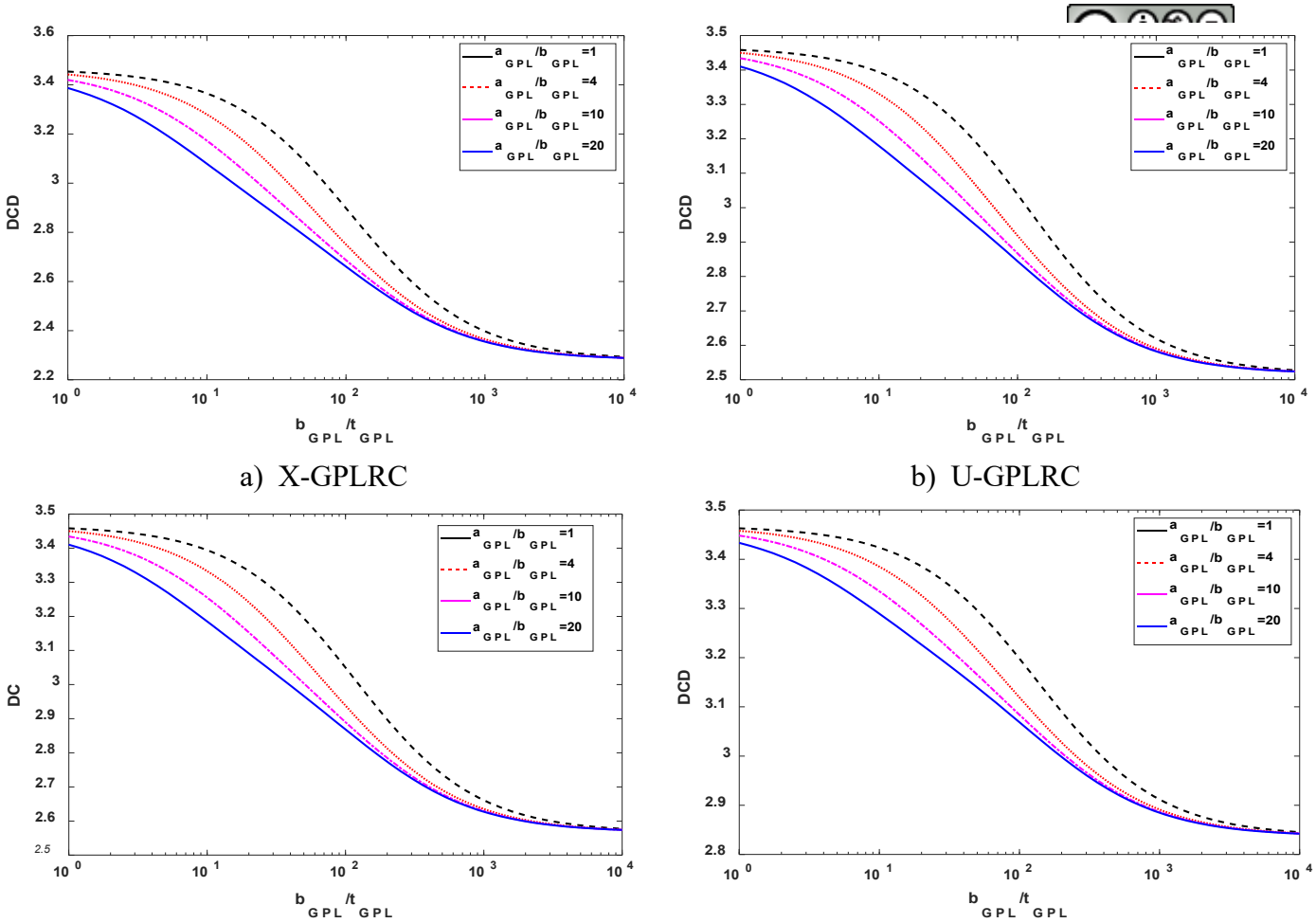

a) X-GPLRC

b) U-GPLRC

c) A-GPLRC

d) O-GPLRC

Figure 5: Effects of GPL geometry and dimension on the deflection of GPLRC C-C beams ($GG/h = 10$, $WW_{GGGGGG} = 0.1\%$, $aa_{GGGGGG} = 2.5\text{x}10^{-6}$)

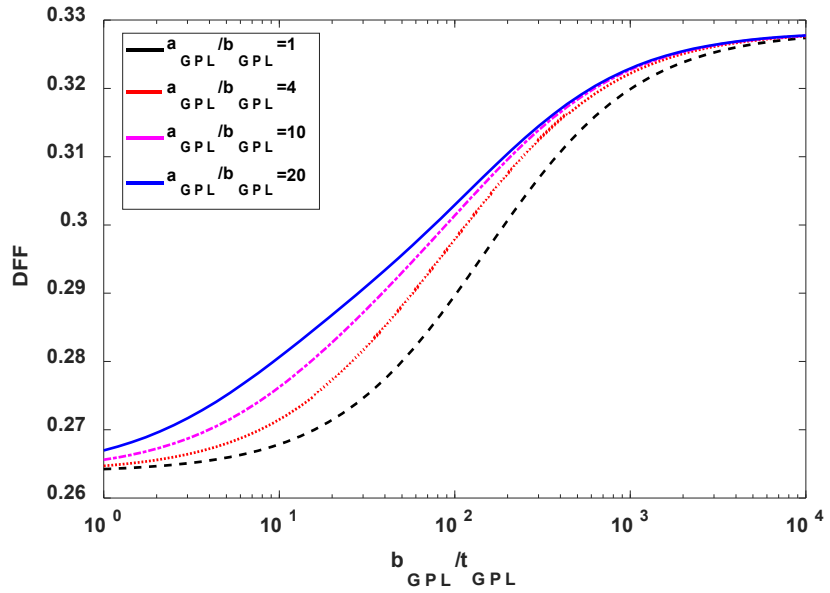

a) Fundamental frequency

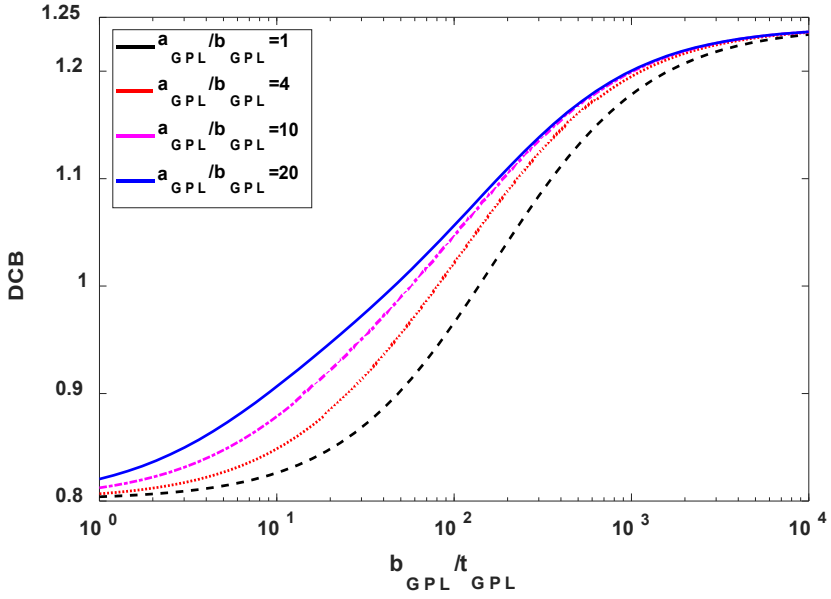

b) Critial buckling loads

Figure 6: Effects of GPL geometry and dimension on the natural frequencies and critical buckling loads of X-GPLRC S-S beams ($GG/h = 10$, $WW_{GGGGGG} = 0.1\%$, $aa_{GGGGGG} = 2.5\text{x}10^{-6}$)

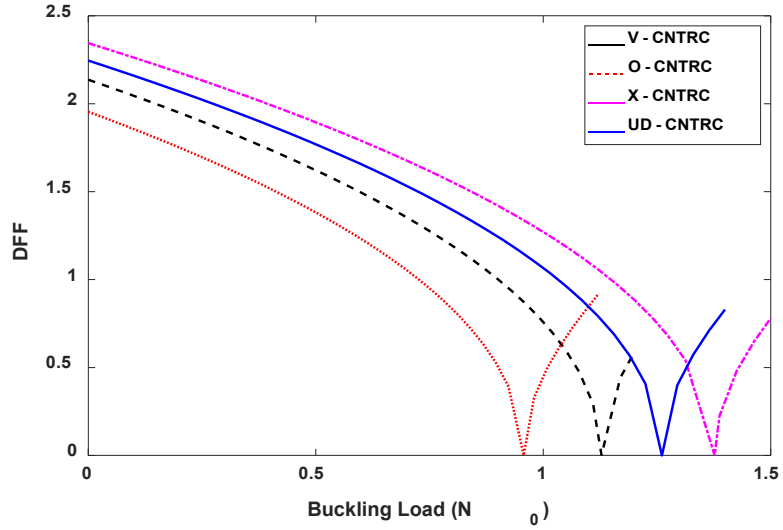

a. CNTRC beams ($V^*_{cn} = 0.17$)

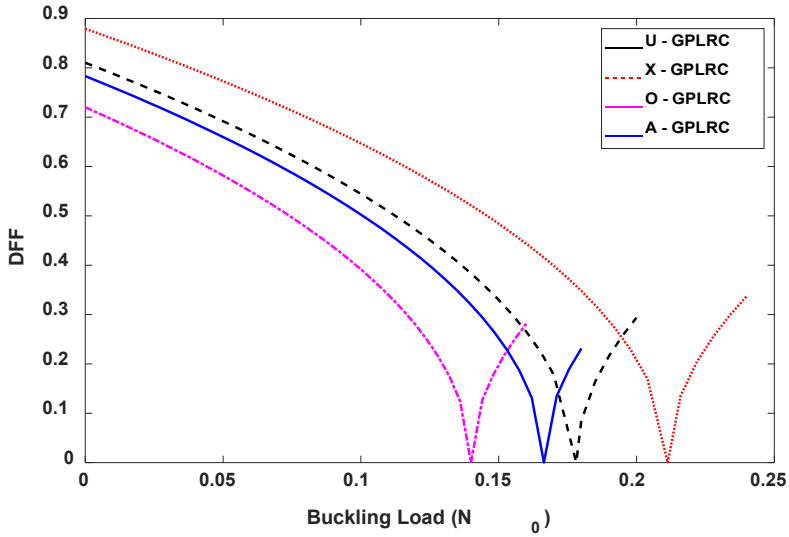

b. GPLRC beams ($WW_{GGGGG} = 0.3\%$)

Figure 7. Load-frequency curve of CNTRC and GPLRC C-C beams ($GG/h = 10$)

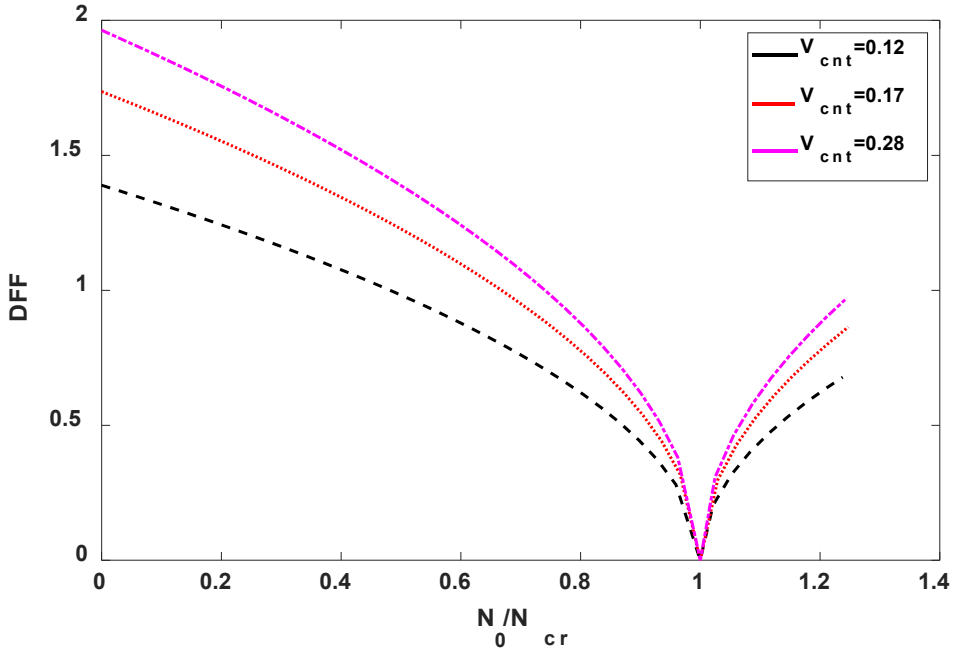

a. X-CNTRC beams

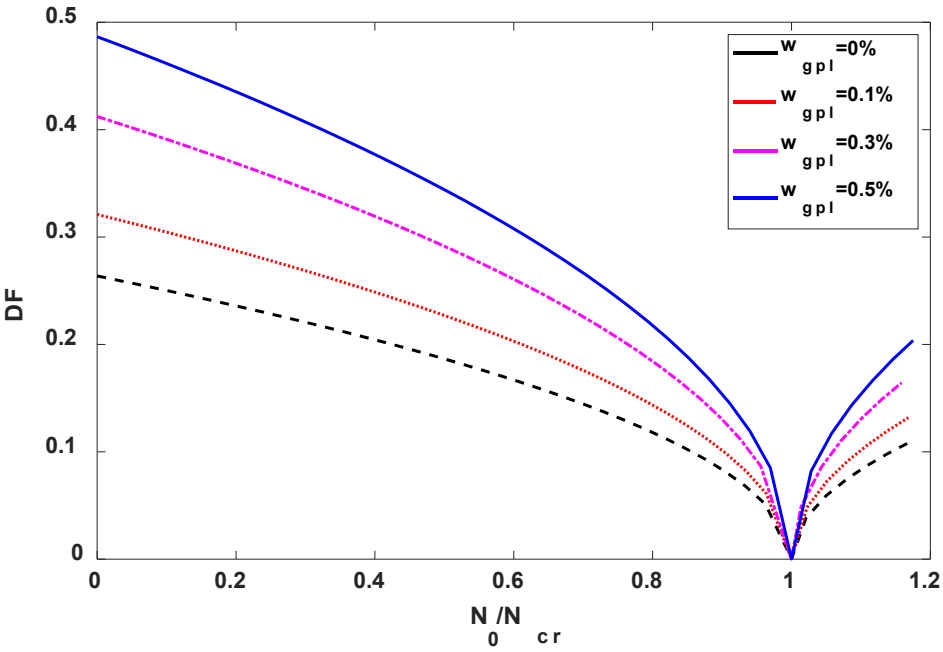

b. X-GPLRC beams

Figure 8. Load-frequency curve of X-CNTRC and X- GPLRC S-S beams ($\mathbb{G}/h = 10$)

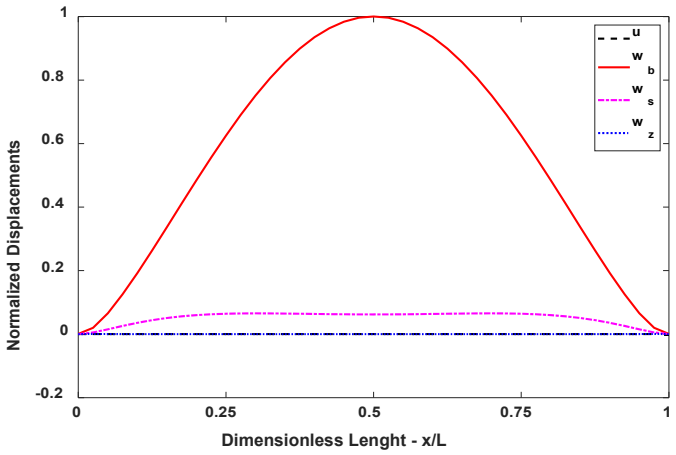

a) $CC_0/CC_{cccc} = -0.5$

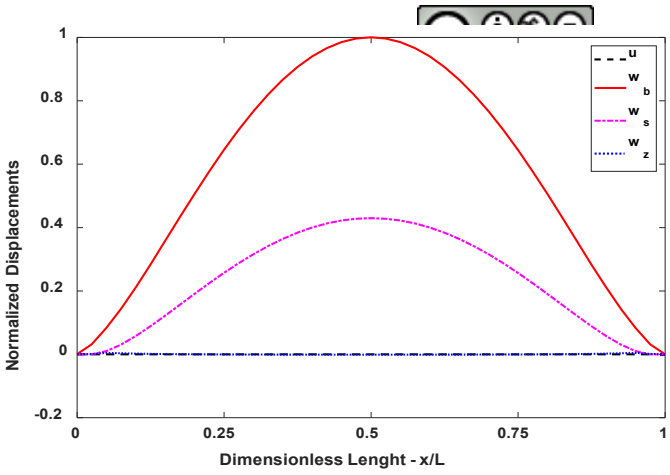

a) $CC_0/CC_{cccc} = -0.5$

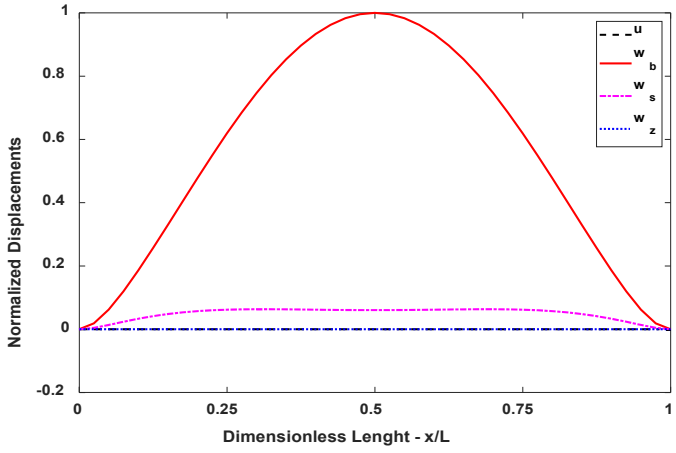

b) $CC_0/CC_{cccc} = 0$

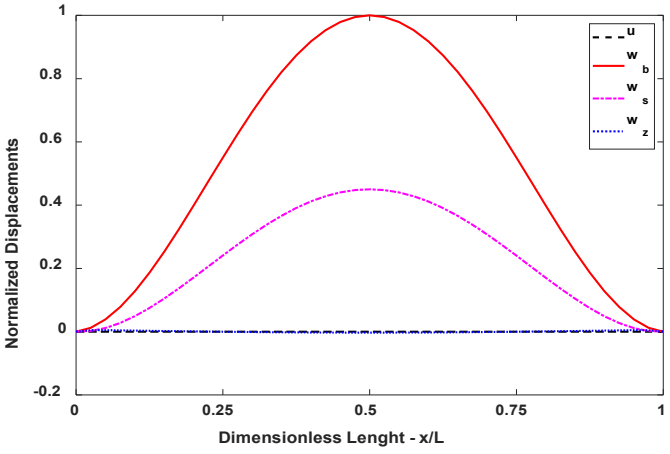

b) $CC_0/CC_{cccc} = 0$

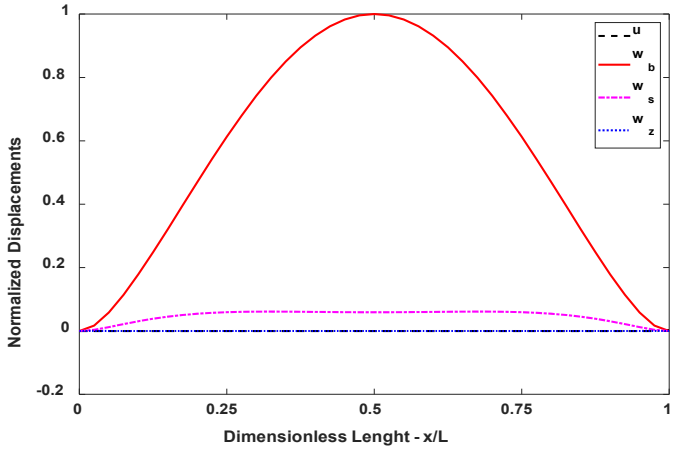

c) $CC_0/CC_{cccc} = 0.5$

X-CNTRC

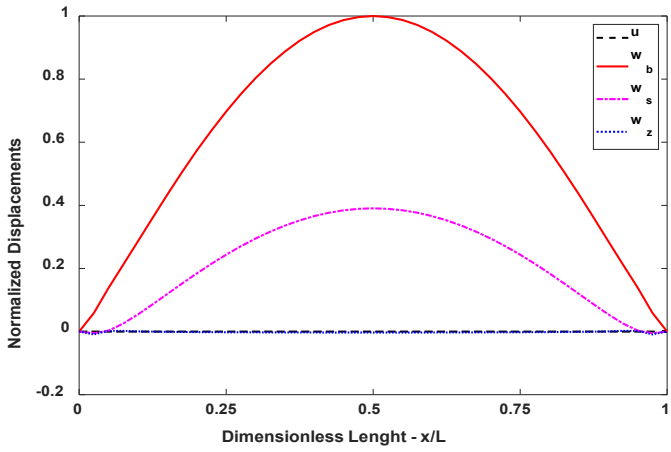

c) $CC_0/CC_{cccc} = 0.5$

X- GPLRC

Figure 9. Vibration mode shapes of X-CNTRC and X- GPLRC C-C beams ($GG/h = 10$, $WW_{GGGGGG} = 0.3\%, VV^*_{CCCCC} = 0.17$)